Economic Geology
Vol. 95, 2000, pp. 1155–1164

SCIENTIFIC COMMUNICATIONS

TEMPORAL EVOLUTION OF ARC MAGMATISM AND HYDROTHERMAL ACTIVITY, INCLUDING EPITHERMAL GOLD VEINS, BOROVITSA CALDERA, SOUTHERN BULGARIA

BRAD SINGER†
Department of Geology and Geophysics, University of Wisconsin-Madison, 1215 West Dayton St., Madison, Wisconsin 53706

AND PETER MARCHEV
Geological Institute, Bulgarian Academy of Sciences, Acad. G. Bonchev Str. bl. 24 Sofia 1113, Bulgaria

Abstract

Plutonic, volcanic, and hydrothermal activity in magmatic arcs is commonly focused spatially, leaving behind complex records of multiple ore-forming processes that can be appreciated in detail only if the timing of igneous and hydrothermal systems is ascertained. The Spahievo ore district, Bulgaria, is adjacent to the Oligocene Borovitsa caldera, one of the largest in Europe. Juxtaposition of porphyry mineralization, barren advanced argillic alteration, and low-sulfidation epithermal alteration and mineralization zones along the caldera margin provides an uncommon opportunity to examine the temporal development of an evolved magmatic-hydrothermal system. $^{40}Ar/^{39}Ar$ ages determined using a CO_2 laser to fuse or incrementally heat minerals from fresh igneous and altered rocks indicate a rapid succession of (1) pre-caldera intermediate magmatism including monzonitic intrusion and coeval porphyry-style mineralization and advanced argillic alteration between 32.9 and 32.3 Ma; (2) rhyolitic ash-flow tuffs, dikes, and domes, with adularia-sericite alteration accompanied by epithermal precious metal mineralization at 32.1 Ma; and (3) nearly synchronous collapse of a nested caldera and intrusion of a ring-fault rhyolite dome and intracaldera dikes at 31.8 Ma. These ages link monzonitic intrusion, Cu-Mo mineralization, and advanced argillic alteration, and indicate that rhyolitic magmatism and adularia-sericite alteration with associated base-metal plus Au mineralization is slightly younger, about 100 to 500 k.y. Deposition of Au ore ca. 300 k.y. prior to caldera collapse distinguishes this ore district from many well-known deposits in which ore formation accompanied andesitic or rhyolitic intrusions along ring fractures that postdate the collapse.

Introduction

The great variety of Cu, Mo, and base and precious metal ores formed in the proximity of plutons or volcanic complexes in continental magmatic arcs reflects interactions between a broad range of potential magma types and heterogeneous host rocks and fluids (Hedenquist and Lowenstern, 1994; Hedenquist et al., 1996). Bonham (1986), Sillitoe (1989), and Hedenquist et al. (1996) reviewed generalized associations of porphyry and high-sulfidation (acid-sulfate) type ore deposits with andesitic to dacitic intrusions, and low-sulfidation (adularia-sericite) Au deposits with andesitic and rhyolitic magmatism. Critical to determining the origin of these ore deposits is establishing temporal, as well as spatial, relations between magmatic and hydrothermal systems. Only recently, for example, through precise K-Ar and $^{40}Ar/^{39}Ar$ dating, was the genetic connection between porphyry and high-sulfidation ore deposits confirmed at Lepanto-Far Southeast, Philippines (Arribas et al., 1995a; Hedenquist et al., 1998) and Cobre Potrerillos, Chile (Marsh et al., 1998). In these and other porphyry deposits, the processes forming K silicate to sericite alteration were related and at Lepanto-Far Southeast occurred over about 100 k.y. (Hedenquist et al., 1998). In contrast, it has been more difficult to relate adularia-sericite deposits to specific magmas because they typically form distal to intrusions, with some hydrothermal systems apparently persisting up to 1.5 m.y. after volcanism (Silberman, 1985; Heald et al., 1987; Hedenquist and Lowenstern, 1994; Conrad and McKee, 1996).

Districts that preserve both low- and high-sulfidation alteration and mineralization provide opportunities to probe the temporal evolution and genesis of complex epithermal systems and their magmatic roots (e.g., Love et al., 1998). Limited K-Ar and $^{40}Ar/^{39}Ar$ dating suggests age differences between the two alteration types that range from 300 to 800 k.y. in the Plio-Pleistocene Baguio volcano, Philippines and the Tavua caldera, Fiji (Setterfield et al., 1992; Aoki et al., 1993), and up to 1.6 m.y. in the Eocene Mount Skukum Au deposit, Yukon Territory, Canada (Love et al., 1998).

One of the major metallogenic provinces of southeastern Europe is the Rhodope massif of Bulgaria and Greece, comprising, in part, Paleogene intrusive and volcanic rocks (Fig. 1a), numerous epithermal base- and precious-metal ore deposits, and several small porphyry Cu-Mo systems. Georgiev et al. (1996) and Arikas and Voudouris (1998) describe the close spatial relationships between porphyry stocks of intermediate composition and porphyry alteration-mineralization, and between rhyolitic magmatism and low-sulfidation base- and precious-metal mineralization. These deposits provide the opportunity to delineate the temporal and chemical evolution of magma-driven hydrothermal systems from porphyry through high-sulfidation and low-sulfidation deposits. However, precise ages and genetic relations between specific

† Corresponding author: e-mail, bsinger@geology.wisc.edu

0361-0128/00/3080/1155-10 $6.00

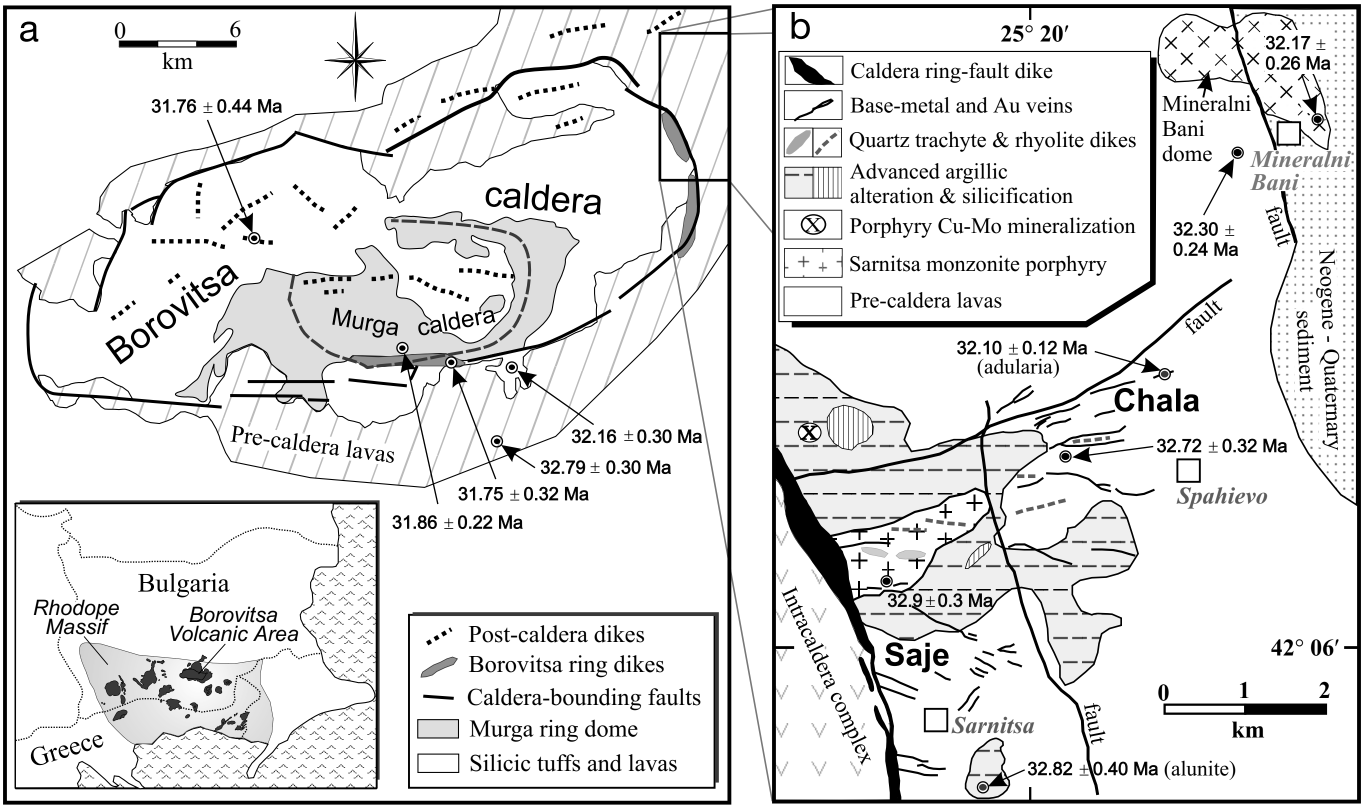

FIG. 1. a. Map of the Borovitsa volcanic area, showing location and ages of samples outside the Spahievo ore district. Paleogene intrusive and volcanic areas in the Rhodope massif (inset) are highlighted. b. Simplified geologic map of the Spahievo ore district, showing sample locations and ages (modified after Ivanov, 1972).

magmatic, alteration, and mineralization events are unknown. The timing and significance of caldera formation with respect to magmatic evolution and mineralization in the larger Rhodope magmatic systems (Fig. 1a) are also unclear.

We report $^{40}Ar/^{39}Ar$ laser-fusion and incremental heating ages of minerals in fresh and altered rocks encompassing the major structural, magmatic, and hydrothermal events in the Spahievo ore district. We focused on this district because (1) it contains alteration styles from porphyry through advanced argillic to adularia-sericite spanning those observed in the Rhodope massif; (2) unusually close and unambiguous spatial relationships between fresh magmatic rocks and the major types of alteration and mineralization are preserved; and (3) definite structural and temporal relations with large-scale caldera magmatism are evident. Our results imply a succession of igneous intrusions, at least two hydrothermal systems, and a major caldera collapse over a period of about 1 m.y.

Geologic Setting, Hydrothermal Activity, Alteration and Mineralization

The Borovitsa volcanic area is the largest (1,150 km^2) volcanic complex within an Eocene-Oligocene continental magmatic arc that extended from Serbia and Macedonia in the northwest to western Anatolia in the southeast (Fig. 1a). The arc is characterized by fault-controlled magmatism in a predominantly extensional setting. Fault orientation varies from northwest-southeast in the west to east-west in the east (Kharkovska, 1984). The Spahievo ore district is located 180 km southeast of Sofia adjacent to the northeast margin of Borovitsa caldera (Fig. 1b). The geology of the district is known from detailed mapping, geophysics, drilling and reconnaissance K-Ar dating (Ivanov, 1972; Marchev, 1985; Yosifov et al., 1990; Yanev and Pėcskay, 1997). Shoshonitic basalt to high silica rhyolite, including lava flows, pyroclastic rocks, stocks, and dikes, were intruded into local pre-Mesozoic basement (Marchev, 1985). Volcanism progressed through three stages (Ivanov, 1972) beginning ~34 Ma (Z. Pėcskay, pers. commun., 1998 unpub. K-Ar data):

1. ~300 km^3 of pre-caldera lavas were erupted consisting of shoshonite and latite with minor high-alumina basalt and absarokite. Magmas became more silicic with time, culminating in ~1,000 km^3 of trachytic, latitic, and rhyolitic pyroclastic rocks, lava flows, and domes.
2. The collapse of two nested calderas, the older, 7 × 7 km Murga and younger, 30 × 15 km Borovitsa, was followed by emplacement of high and low silica rhyolites (quartz trachytes) along caldera-related ring fractures.
3. Finally, shoshonitic mafic to silicic stocks and dikes intruded through intracaldera tuffs and Murga caldera-rim rhyolites (Fig. 1a).

The Spaheivo ore district is hosted by a 1,000-m-thick sequence of precaldera porphyritic latite lavas (Ivanov, 1972; Yanev and Pėcskay, 1997). Numerous igneous stocks, some inferred through geophysics, intrude the local precaldera volcanic sequence (Yosifov et al., 1990). For example, the magnetic signature of the Sarnitsa intrusion suggests that its subsurface volume to the north and southeast may be several times that which might be inferred from the small outcrop area of 1.5 km^2 (Yosifov et al., 1990). From the estimated thickness of the overlying volcanic sequence, the original depth of the intrusion's top was ca. 1 km (Fig. 2). East-west quartz trachyte and high silica rhyolite dikes cut the Sarnitsa intrusion and its host rocks, whereas quartz trachyte ring dikes, intruded along bounding faults associated with collapse of the Borovitsa caldera, cut the western part of the intrusion (Fig. 1b; Ivanov, 1972). The magnetic properties of a subjacent, possibly down-dropped, portion of the intrusion were detected to the west, 1 km beneath rhyolitic intracaldera tuff (Fig. 2; Yosifov et al., 1990). These observations indicate that the Sarnitsa intrusion is older than the Borovitsa caldera.

The major alteration and mineralization events in the Spaheivo ore district are closely associated with the Sarnitsa intrusion and silicic dikes (Figs. 1b and 2). Following the intrusion, a porphyry-style hydrothermal system produced subeconomic Mo-Cu mineralization 1 km to the north (Fig. 1b). The highest bulk Cu (800 ppm) and Mo (370 ppm) contents define a 250 m by 200 m surface anomaly (marked X in Fig. 1b) that is located within a zone of quartz-sericite-pyrite ± alunite and diaspore alteration where Cu is concentrated in turquoise (Kunov, 1987). Several drill holes reached primary Cu-Mo mineralization consisting of molybdenite, chalcopyrite, and bornite in quartz veinlets less than 0.5 cm wide at depths of several meters. Minor white mica occurs as intergrowths with the molybdenite crystals. The mineralization is concentrated in precaldera lava flows; however, some drill cores penetrated mineralized monzonite of the intrusion as well. Alteration at depth comprises quartz-pyrophyllite-diaspore-illite with minor kaolinite and alunite. K silicate alteration typical of deeper parts of porphyry systems was not encountered in the drill holes, although biotite-albite alteration occurs along the northeast contact of the intrusion (Mavroudchiev and Botev, 1966; Kunov, 1987, 1991). Thus, the advanced argillic alteration was either superimposed on the Sarnitsa Cu-Mo stockwork (e.g., Sillitoe, 1995), or formed contemporaneously with sericitic alteration similar to Lepanto-Far Southeast (Hedenquist et al., 1998). Typical of the lithocaps that form over porphyry deposits (Sillitoe, 1995), this advanced argillic alteration grades upward into a resistant quartz-alunite carapace (Kunov, 1991) that crops out 300 m east of the Cu-Mo anomaly and 2 km south of the Sarnitsa intrusion, near the dated alunite sample (Fig. 1b). Unlike several Tertiary examples (e.g., Heald et al., 1987), the advanced argillic zone is barren—this may reflect insufficient fracturing to focus later ascending ore solutions (Hedenquist et al., 1998).

A hydrothermal system developed following intrusion of the high silica rhyolite dikes and produced the Saje base-metal and Chala Au epithermal deposits within and adjacent to the Sarnitsa intrusion (Fig. 1b). Epithermal mineralization, hosted in breccias and veins, shows a crude vertical zonation from chalcopyrite-galena-sphalerite-quartz in Saje deposit to quartz-specularite-adularia and Au in the Chala deposit. The Saje deposit is closer to the caldera rim (Fig. 1b) and most probably represents a deeper erosional level than the Chala deposit, which is characterized by a cap of massive silicification. Moreover, the quartz-kaolinite O isotope thermometer suggests that at Chala silicification occurred at 150°C (McCoyd, 1985), typical of relatively shallow steam-heated zones in modern geothermal fields (Hedenquist, 1990). The epithermal veins are closely associated with the high silica

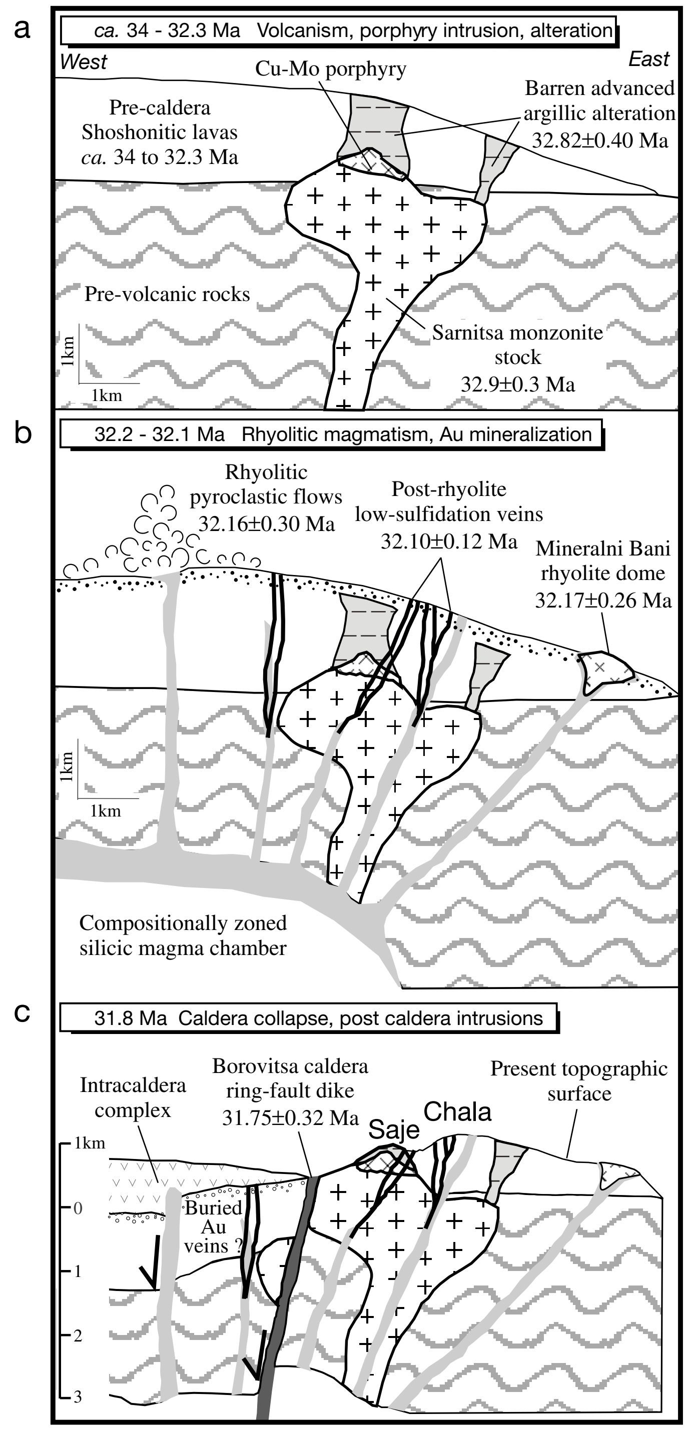

FIG. 2. Generalized west-east cross sections illustrating development of Spaheivo ore district.

rhyolite dikes and both are radial to the Borovitsa caldera (Figs. 1b and 2). Some veins crosscut the Sarnitsa intrusion and argillic alteration, indicating that low sulfidation mineralization is younger than these features. Adularia-sericite alteration forms extensive envelopes tens of meters wide around veins with an innermost quartz-adularia zone surrounded by quartz-sericite and propylitic zones. The low-sulfidation veins are, like the Sarnitsa intrusion, cut by the ring dike associated with collapse of the Borovitsa caldera (Fig. 1b; Ivanov, 1972), indicating that Au deposition preceded caldera collapse. Cores drilled by the Bulgarian Geoengineering Enterprise in the early 1990s suggest an Au resource at Chala of 20 t at a grade of 8 g/t, including bonanza grades to 600 g/t at shallow depths.

$^{40}Ar/^{39}Ar$ Methods, Samples, and Results

$^{40}Ar/^{39}Ar$ experiments were undertaken on separates of K feldspar, biotite, sanidine, plagioclase, alunite, and adularia from 12 rocks purified by crushing, sieving to 100–250 μm, and hand-picking. Several milligrams of each mineral were irradiated at Oregon State University for 12 or 50 hours. The neutron fluence monitor was 27.92 Ma sanidine from the Taylor Creek rhyolite (Duffield and Dalrymple, 1990). Degassing involved fusing sub-milligram aliquots for 60 s with a 25W CO_2 laser. Following 2 to 5 min of clean-up on SAES getters, the isotopic composition of gas from each fusion or heating step was measured using an MAP 216 spectrometer. Analytical and data reduction procedures are discussed in Singer et al. (1999). Fusion analyses were performed on 4 to 13 individual aliquots from each sample and from these, arithmetic mean ages, inverse-variance weighted mean ages, and 2σ uncertainties were calculated (Table 1; Appendix). Weighted mean ages and errors are preferred because imprecise data has less impact on determining the most reliable ages. In addition, 1.8 and 3.0 mg of the adularia and alunite were incrementally heated in 11 and 7 steps, respectively, using a CO_2 laser with a faceted objective lens to deliver a 9 mm^2 beam and evenly heat the samples (Table 2). The resulting age spectra are illustrated in Figure 3.

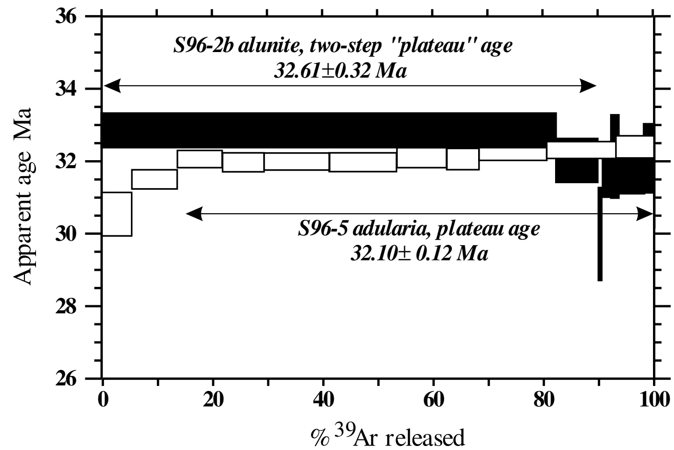

FIG. 3. Age spectrum diagram of $^{40}Ar/^{39}Ar$ incremental heating results from alunite and adularia samples typical of high- and low-sulfidation alteration at Spaheivo ore district.

Precaldera magmatism and alteration

Ages for precaldera magmatic activity were determined from three lava flows (S96-4, 208, and S96-11), the extensive Borovitsa rhyolite tuff (Br97-3) from the edge of the caldera, and the high silica rhyolite dome of Mineralni Bani (Br97-2) (Table 1; Fig. 1). Fresh K feldspar and biotite from an unaltered portion of the intrusion gave identical ages of 32.99 ± 0.38 Ma and 32.85 ± 0.28 Ma, implying rapid cooling below their closure temperatures of ~350° to 150°C (McDougall and Harrison, 1999). Sanidine from a high K latite gave an age of 32.72 ± 0.32 Ma, indistinguishable from that of the intrusion. The age of 32.30 ± 0.24 Ma from latite lava near Mineralni Bani constrains the end of intermediate volcanism, whereas slightly younger silicic volcanism is recorded by an adjacent rhyolite dome and eruption of several 100 km^3 of trachytic to mainly rhyolite tuff at 32.17 ± 0.26 Ma and 32.16 ± 0.32 Ma, respectively (Figs. 1 and 4).

TABLE 1. Summary of $^{40}Ar/^{39}Ar$ Age Determinations from 105 Laser-Fusion Experiments on 12 Spaheivo Ore District Units

Sample	Mineral	Description	Number of fusions	Simple mean age[1] Ma ± 2σ	Weighted mean age[2] Ma ± 2σ
224	Sanidine	Postcaldera quartztrachyte dike	7	31.72 ± 0.28	31.75 ± 0.32
B86-37	Biotite	Postcaldera melalatite dike	7	31.66 ± 1.08	31.76 ± 0.44
217A	Sanidine	Murga caldera, rhyolite ring-dike	10	31.87 ± 0.36	31.86 ± 0.22
Zd-95-1	Plagioclase	Borovitsa caldera rhyolite tuff (outflow)	4	31.89 ± 0.32	31.93 ± 0.50
S96-5	Adularia	Low-sulfidation alteration, Chala vein no. 8	8 of 11[3]	32.13 ± 0.20	32.12 ± 0.14
Br97-3	Sanidine	Pre-Borovitsa caldera pyroclastic flow	8 of 9[3]	32.17 ± 0.34	32.16 ± 0.30
Br97-2	Sanidine	Mineralni Bani rhyolite dome	8	32.17 ± 0.26	32.17 ± 0.26
S96-11	Sanidine	Mineralni Bani latite flow	8	32.30 ± 0.28	32.30 ± 0.24
S96-4	Sanidine	Precaldera, high K latite lava	7	32.71 ± 0.40	32.72 ± 0.32
208	Biotite	Precaldera lava	4	32.80 ± 0.40	32.79 ± 0.30
S96-2b	Alunite	High-sulfidation alteration	13	32.82 ± 1.06	32.82 ± 0.40
S96-1	Biotite	Sarnitsa monzonite intrusion	6	32.85 ± 0.30	32.85 ± 0.28
S96-1	K feldspar	Sarnitsa monzonite intrusion	7	32.92 ± 0.78	32.99 ± 0.38

Individual sub-samples of each mineral were between 0.1 to 1.0 mg in size
[1] Ages calculated relative to 27.92 Ma TCR-Sanidine, ±2σ errors; λ_E = 0.581 × 10^{-10}/yr; λ_B = 4.692 × 10^{-10}/yr (see text)
[2] Error-weighting is by the inverse of the variance; weighted mean ages are preferred as they emphasize more radiogenic analyses
[3] Outliers beyond 95% confidence interval about the mean age were excluded from age determinations

TABLE 2. $^{40}Ar/^{39}Ar$ Incremental-Heating Analyses of Adularia and Alunite Samples from Spaheivo

Percent laser power	$^{40}Ar/^{39}Ar$	$^{37}Ar/^{39}Ar$[1]	$^{36}Ar/^{39}Ar$	$^{40}Ar^*$ (10^{-14} mole)	% $^{40}Ar^*$	K/Ca	% ^{39}Ar	Apparent age ± 2σ Ma[2]
S96-5 Adularia (1.8 mg)		J = 0.01293						
10	3.425	0.00419	0.0071032	0.990	38.6	116.97	5.01	30.57 ± 0.58*
11	1.805	0.00388	0.0014827	1.790	75.5	126.38	8.85	31.41 ± 0.26*
12	1.634	0.00392	0.0008347	1.640	84.7	125.10	7.94	32.08 ± 0.20
13	1.670	0.00415	0.0009537	1.520	82.9	118.17	7.37	31.99 ± 0.24
15	1.719	0.00409	0.0011151	2.530	80.6	119.72	12.30	32.02 ± 0.22
17	1.755	0.00321	0.0012425	2.450	78.8	152.69	11.92	31.99 ± 0.24
20	1.714	0.00368	0.0010869	1.850	81.0	133.01	8.94	32.11 ± 0.26
22	1.789	0.00580	0.0013470	1.240	77.5	84.42	6.02	32.07 ± 0.28
24	1.751	0.00394	0.0011876	2.520	79.7	124.23	12.16	32.27 ± 0.26
26	1.801	0.00400	0.0013523	2.620	77.6	122.44	12.60	32.30 ± 0.24
30	1.845	0.00413	0.0014853	1.430	76.0	118.55	6.89	32.41 ± 0.26
				Weighted mean plateau age				32.10 ± 0.12
S92-2b Alunite (<3 mg)		J = 0.01302						
10	2.808	0.01574	0.0047550	7.710	50.0	7.22	82.23	32.87 ± 0.38
12	2.833	0.06166	0.0049304	0.740	48.6	7.94	7.69	32.04 ± 0.56
12.5	3.345	0.06363	0.0069704	0.007	38.5	7.70	0.79	29.97 ± 1.28*
13.5	2.715	0.05068	0.0045750	0.145	50.2	9.67	1.51	31.73 ± 0.66*
15	3.562	0.06061	0.0073940	0.145	38.7	8.08	1.49	32.05 ± 1.10*
17.5	3.474	0.05623	0.0071257	0.440	39.4	8.71	4.56	31.86 ± 0.72*
20	3.476	0.04951	0.0070981	0.168	39.6	9.90	1.73	32.09 ± 0.88*
				Weighted mean, "two-step" plateau age				32.61 ± 0.32

Heating was via a 25W CO_2 laser and faceted lens to spread the beam over a 9 mm^2 spot
Reactor corrections: $^{36}Ar/^{37}Ar(Ca)$ = 0.0000268, $^{39}Ar/^{37}Ar(Ca)$ = 0.000698, and $^{40}Ar/^{39}Ar(K)$ = 0.0465
[1] Corrected for ^{37}Ar and ^{39}Ar decay, half-lives of 35 days and 259 years, respectively
[2] Ages calculated relative to TCR-sanidine (27.92 Ma; Duffield and Dalrymple, 1990; see text), ± 2σ errors
$\lambda_E = 0.581 \times 10^{-10}$/yr; $\lambda_B = 4.692 \times 10^{-10}$/yr; weighting for means is by the inverse of the variance
*Indicates step not used in plateau age calculation

The timing of advanced argillic alteration was obtained by dating alunite (S96-2b) from barren alteration 2 km south of Sarnitsa intrusion (Fig. 1b). Thirteen laser fusion experiments gave a weighted mean age of 32.82 ± 0.40 Ma, whereas the incremental-heating age spectrum is discordant. The first two steps comprising 90 percent of the gas define a two-step "plateau" age of 32.61 ± 0.32 Ma, identical with the fusion results (Figs. 3 and 4). Since it is difficult to control sample temperature with the laser, the apparently younger, high-temperature steps comprising 10 percent of the gas may simply reflect quantitative degassing of radiogenic argon from alunite via dehydroxylation reactions at <550°C (Itaya et al., 1996; Love et al., 1998). Though lacking a plateau by more formal definitions (e.g., McDougall and Harrison, 1999), the age spectrum is important in that it shows no evidence for diffusive loss of argon via heating or alteration following formation of the alunite. In fact, the fusion and "plateau" ages are indistinguishable from those obtained for the Sarnitsa monzonite (Fig. 4).

The age of alteration associated with the low-sulfidation Chala ores was obtained from adularia in the altered latite lava hosting zone 3 of the deposit. Eight total fusions gave a weighted mean of 32.12 ± 0.28 Ma, concordant with the more precise plateau age of 32.10 ± 0.12 Ma given by 85 percent of the gas released by incremental heating (Fig. 3). We take the plateau as the most reliable age for the alteration and associated low-sulfidation Au deposition.

Murga and Borovitsa calderas and postcaldera volcanism

Sanidine from the Murga caldera rhyolite dome (sample 217) yielded a total fusion age of 31.86 ± 0.22 Ma. It is intruded by a less silicic quartz trachyte dike (224) of the Borovitsa caldera ring-fault system, with sanidine dated at 31.75 ± 0.34 Ma (Figs. 1a and 4). In addition, biotite from a mafic dike that crosscuts welded intracaldera ignimbrites gave an identical age of 31.76 ± 0.44 Ma (Table 1). The resurgent rhyolite dome of the Murga caldera is cut by ring dikes associated with collapse of the Borovitsa caldera (Fig. 1a), thereby predating the Borovitsa caldera. Our $^{40}Ar/^{39}Ar$ results indicate that collapse and resurgence of the Murga caldera, collapse of the Borovitsa caldera, and postcollapse intrusion of chemically bimodal dikes occurred over a period that was less than the resolution of the dating method, i.e., <400 k.y. The arithmetic mean of these three virtually identical age determinations suggests that this rapid succession of events took place at 31.79 ± 0.08 Ma, approximately 300 ± 200 k.y after alteration associated with the low-sulfidation Au deposition (Fig. 4). Plagioclase in outflow tuff 18 km south of the Borovitsa caldera margin gave a less precise age of 31.93 ± 0.50 Ma (Table 1), consistent with the 31.79 ± 0.08 Ma age bracket on caldera collapse.

Discussion and Implications

Our $^{40}Ar/^{39}Ar$ results indicate that the duration of magmatism and associated hydrothermal activity was most probably

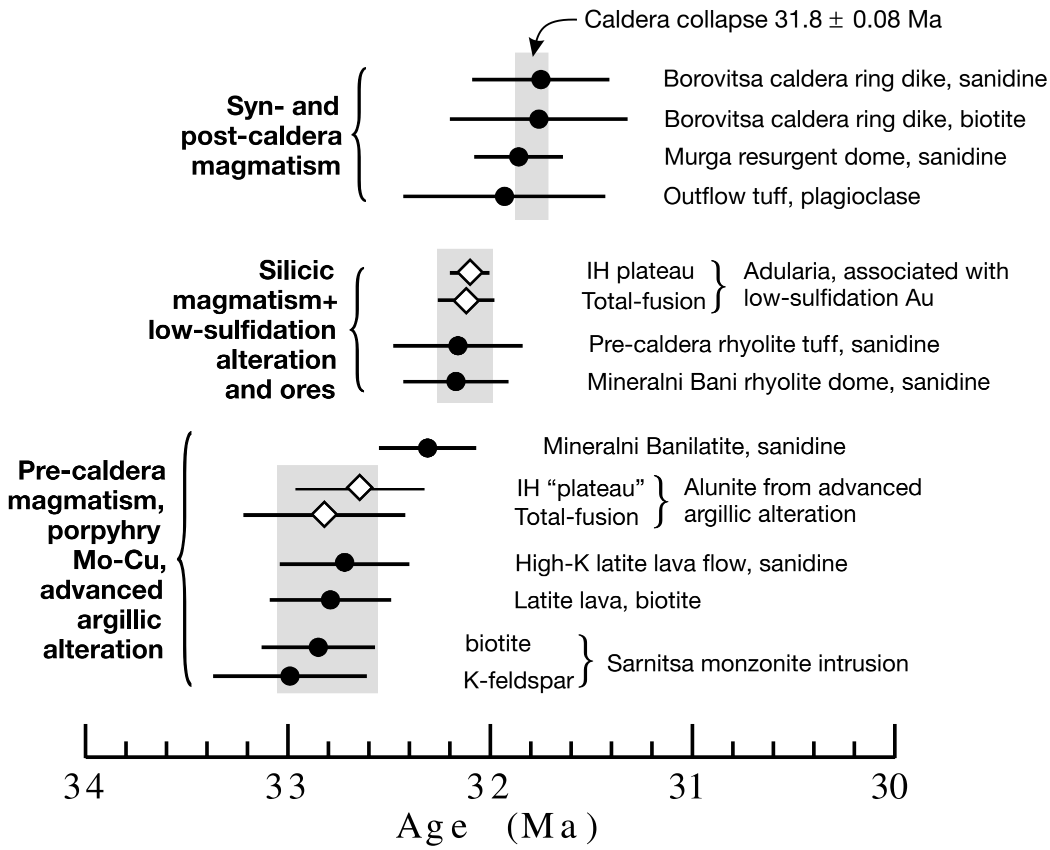

FIG. 4. Summary of $^{40}Ar/^{39}Ar$ laser-fusion and incremental-heating age determinations from fresh and altered rocks in the Spaheivo ore district and Borovitsa volcanic area. Vertical gray bands delinate most probable ages for the three episodes described at left. Shown are weighted mean or plateau ages; uncertainties $\pm 2\sigma$.

between 0.5 and 1.0 m.y. (Fig. 4). The hydrothermal systems that formed advanced argillic and adularia-sericite alteration, the latter hosting low-sulfidation epithermal Au ore, were spatially distinctive and reflect transport of strongly contrasting fluid compositions in systems separated by not less than 100 k.y., but more likely about 500 k.y. (Fig. 4). Like the well-dated Potrerillos and Lepanto-Far Southeast systems (Marsh et al., 1997; Hedenquist et al., 1998), early porphyry mineralization and associated advanced argillic alteration in the Spahievo ore district reflects a coeval magmatic-hydrothermal system that probably lasted on the order of 100 to 300 k.y.

Vein-hosted base-metal and Au mineralization followed the Sarnitsa intrusion by only 300 to 800 k.y. (Fig. 2). However, numerical modeling (Cathles et al., 1997; Marsh et al., 1997; Shinohara and Hedenquist, 1997) indicates that shallow stocks 1 to 2 km in diameter cool below the closure temperature of dateable minerals in «100 k.y. Thus, it is highly unlikely that the Sarnitsa intrusion was the heat source for the much younger low-sulfidation alteration and mineralization. Rather, the low-sulfidation alteration was intimately associated with rhyolite dikes and their identical $^{40}Ar/^{39}Ar$ ages further suggest that rhyolitic magmas and hydrothermal processes leading to low-sulfidation mineralization were genetically related. Moreover, multidomain thermal modeling (Henry et al., 1997) of flat adularia age spectra remarkably similar to that in Figure 4 suggests that these Au-bearing veins were emplaced rapidly and is inconsistent with a longevity of hydrothermal circulation for a period in excess of uncertainty in the plateau age, or about 120 k.y. We propose that the source of the rapidly emplaced rhyolite domes, dikes, precaldera tuffs, and brief low-sulfidation hydrothermal activity was a rhyolite-capped magma chamber at depths of 3 to 5 km, similar to that underlying many calderas (Fig. 2b; Lipman, 1992).

Although low-sulfidation mineralization typically postdates rhyolitic magmatism by several hundred k.y. and possibly more than 1 m.y. (Silberman, 1985; Heald et al. 1987; Conrad and McKee, 1996), Henry et al. (1997) demonstrated that at Round Mountain, Nevada, large, low- sulfidation Au deposits can form rapidly, on the order of 50 to 100 k.y. The Chala deposit is similar, having formed rapidly after rhyolitic intrusion. Like the Chala deposit, Au ore at Round Mountain is intimately related to caldera magmatism, although an important distinction is the timing of ore deposition relative to caldera formation. At Round Mountain and most other mineralized calderas in the western United States (Silberman, 1985; Lipman, 1992; Conrad and McKee; 1996; Henry et al., 1997), Au deposition occurred along ring-fracture intrusions that postdated caldera collapse by hundreds of thousands of years and acted as conduits to focus hydrothermal fluid. This also appears to be true at the few other Tertiary (Miocene) calderas in Europe known to be associated with epithermal Au deposits, including the Rodalquilar complex, Spain (Arribas et al., 1995b) and calderas in the Carpathian region (Lexa et al., 1999; Molnár et al., 1999; Prokofiev et al., 1999). Our $^{40}Ar/^{39}Ar$ results indicate that deposition of Au in the Spaheivo ore district was, however, not controlled by the ring fracture of the Borovitsa caldera, since caldera collapse and postcaldera bimodal magmatism occurred ca. 300 k.y. after low- sulfidation ore deposition (Fig. 2).

Field relations coupled with the geochronologic results in the Spahievo ore district indicate a close temporal association of epithermal Au formation with rhyolitic dikes, possibly caused by a genetic relationship, and a rapid succession of magmatic and hydrothermal processes immediately preceding collapse of the adjacent caldera. Our findings suggest that postalteration and mineralization collapse of the chamber roof may have buried and thus preserved portions of the original Au veins in the vicinity of the caldera ring-fracture intrusion. If so, this concept may help guide exploration in this district and in other regions with a similar magmatic and hydrothermal history.

Acknowledgements

Supported at the University of Geneva by the Swiss NSF program for cooperation with Eastern European countries (grant 7BUPJ048659). We thank J.W. Hedenquist, A. Arribas Jr., and F. Molnár for their thorough and helpful comments, A. Kestebekov for field assistance, and R. Raicheva for assistance with the figures.

December 27, 1999; March 20, 2000

REFERENCES

Aoki, M., Comsti, E.C., Lazo, F.B., and Matsuhisa, Y., 1993, Advanced argillic alteration and geochemistry of alunite in an evolving hydrothermal system at Baguio, Northern Luzon, Philippines: Resource Geology, v. 43, p. 155–164.

Arikas, K., and Voudouris, P., 1998, Hydrothermal alterations and mineralizations of magmatic rocks in the southeastern Rhodope massif, *in* Christofides, G., Marchev, P., and Serri, G., eds., Tertiary magmatism of the Rhodopian region: Acta Vulcanologica, v. 10, p. 353–365.

Arribas, A., Jr., Hedenquist, J.W., Itaya, T., Okada, T., Concepción, R.A., and Garcia, J.S., 1995a, Contemporaneous formation of adjacent porphyry and epithermal Cu-Au deposits over 300 ka in northern Luzon, Philippines: Geology, v. 23, p. 337–340.

Arribas, A., Cunningham, C.G., Rytuba, J.J., Rye, R.O., Kelly, W.C., Podwysocki, M.H., McKee, E.H., and Tosdal, R.M., 1995b, Geology, geochronology, fluid inclusions, and isotope geochemistry of the Rodalquilar gold alunite deposit, Spain: ECONOMIC GEOLOGY, v. 90, p. 795–822.

Bonham, H.F., Jr., 1986, Models for volcanic-hosted epithermal precious metal deposits; a review: International Volcanological Congress, Volcanism, Hydrothermal Systems and Related Mineralization, Symposium 5, Auckland, New Zealand, Proceedings, p. 13–17.

Cathles, L.M., Erendi, H.J., and Barrie, T., 1997, How long can a hydrothermal system be sustained by a single intrusive event?: ECONOMIC GEOLOGY, v. 92, p. 766–771.

Conrad, J.E., and McKee, E.H., 1996, High-precision $^{40}Ar/^{39}Ar$ ages of rhyolitic host rocks and mineralized veins at the Sleeper deposit, Humbolt County, Nevada, *in* Coyner, A.R., and Fahey, P.L., eds., Geology and ore Deposits of the American Cordillera: Geological Society of Nevada Symposium Proceedings, Reno/Sparks, Nevada, April 1995, Proceedings, p. 257–262.

Duffield, W. and Dalrymple, G.B., 1990, The Taylor Creek Rhyolite of New Mexico: A rapidly emplaced field of lava domes and flows: Bulletin of Volcanology, v. 52, p. 475–487.

Georgiev, V., Malinov, O., Milovanov, P., and Nikova, L., 1996, Metallogeny of the Spahievo ore field, SE Bulgaria: Plate tectonic aspects of the Alpine metallogeny in the Carpatho-Balkan region. Sofia, UNESCO, IGCP Project N356, v. 2, p. 75–80.

Heald, P., Foley, N.K., and Hayba, D.O., 1987, Comparative anatomy of volcanic-hosted epithermal deposits—acid-sulfate and adularia-sericite types: ECONOMIC GEOLOGY, v. 82, p. 1–26.

Hedenquist, J.W., 1990, The thermal and chemical structure of Broadlands-Ohaaki geothermal system, New Zealand: Geothermics, v. 19, p. 151–185.

Hedenquist, J.W., and Lowenstern, J.B., 1994, The role of magmas in the formation of hydrothermal ore deposits: Nature, v. 370, p. 519–527.

Hedenquist, J.W., Izawa, E., Arribas, A., and White, N.C., 1996, Epithermal gold deposits: Styles, characterstics, exploration: Society of Resource Geology, Tokyo, Japan, Resource Geology Special Publication 1, 18 p.

Hedenquist, J.W., Arribas, A. Jr., and Reynolds, T.J., 1998, Evolution of an intrusion-centered hydrothermal system: Far Southeast-Lepanto porphyry and epithermal Cu-Mo deposit, Philippines: ECONOMIC GEOLOGY, v. 93, p. 373–404.

Henry, C.D., Elson, H.B., McIntosh, W.C., Heizler.M.T., and Castor, S.B., 1997. Brief duration of hydrothermal activity at Round Mountain, Nevada, determined from $^{40}Ar/^{39}Ar$ geochronology: ECONOMIC GEOLOGY, v. 92, p. 807–826.

Itaya, T., Arribas, A., Okada, T., 1996, Argon release systematics of hypogene and supergene alunite based on progressive heating experiments from 100 to 1000° C: Geochimica et Cosmochimica Acta, v. 60, p. 4525–4535.

Ivanov, R. 1972. Volcano-tectonic structures in the Borovitsa depression: Bulletin of the Geological Institute, Studies in Geochemistry Mineralogy and Petrography, v. 21, p. 209–219 (in Bulgarian with English abstract).

Kharkovska, A., 1984, Tertiary magmotectonic zones in Southwest Bulgaria, *in* Magmatism of the Molasse-forming Epoch and its Relation to Endogenous Mineralization: Bratislava, Geologicky Ústav D. Štura, p. 9–34.

Kunov, A., 1987, Mineralogy and zonation of the secondary quartzites from the northeastern periphery of the Borovitsa volcano-tectonic depression: Unpublished Ph.D. thesis, Sofia, Bulgaria, Geological Institute, 220 p.

——1991, Secondary quartzites from the northeastern periphery of the Borovitsa volcanic area. I. Geological-petrographic characteristics of the hydrothermally altered zones: Bulgarian Academy of Sciences, Geochemistry Mineralogy and Petrology, v. 28, p. 46–72.

Lipman, P.W., 1992, Ash-flow calderas as structural controls of ore deposits—recent work and future problems: U.S. Geological Survey Bulletin 2012, p. L1-L12.

Lexa, J., Štohl, J., and Konečnỳ, V., 1999, The Banská Štiavnica ore district: Relationship between metallogenic processes and the geological evolution of a stratovolcano: Mineralium Deposita, v. 34, p. 639–654.

Love, D.A., Clark A.N., Hodgson, C.J., Mortensen, J.K., Archibald D.A, and Farrar E., 1998, The timing of adularia-sericite-type mineralization and alunite-kaolinite-type alteration, Mount Skukun epithermal gold deposit, Yukon Territory, Canada: $^{40}Ar/^{39}Ar$ and U-Pb geochronology: ECONOMIC GEOLOGY, v. 93, p. 437–462.

Marchev, P., 1985, Petrology of the Paleogene volcanics in the area of villages Bezvodno and Rusalsko, Kurdjali district. Unpublished Ph.D. thesis, Sofia, Bulgaria, Sofia University, 327 p.

Marsh, T.M., Einaudi, M.T., and M. McWilliams, 1997, $^{40}Ar/^{39}Ar$ geochronology of Cu-Au and Au-Ag mineralization in the Potrerillos district, Chile: ECONOMIC GEOLOGY, v. 92, p. 784–806.

Mavroudchiev, B., and Botev, S., 1966, Petrology of the Sarnitsa intrusion: Annuaire de l'Université de Sofia, Géologie, v. 59 (2), p. 295–321 (in Bulgarian with German abstract).

McCoyd, R., 1995, Isotopic and geochemical studies of the epithermal-mesothermal Pb-Zn deposits of S.E. Bulgaria: Unpublished Ph.D. thesis, Aberdeen, Scotland, University of Aberdeen, p. 270.

McDougall, I., and Harrison, T.M., 1999, Geochronology and Thermochronology by the $^{40}Ar/^{39}Ar$ method, 2nd edition, New York, Oxford University Press, 269 p.

Molnár, F., Zelenka, T., Mátiás, E., Pècskay, Z., Bajnóczi, B., Kiss, J., and Horváth, I., 1999, Epithermal mineralization of the Tokaj Mountains, northeast Hungary: Shallow levels of low-sulfidation type systems: Society of Economic Geologists Guidebook Series, v. 31, p. 109–153.

Prokofiev, V., Kamenetsky, V.S., Kovalenker, V., Bodon, S.B., and Jelen, S, 1999, Evolution of magmatic fluids at the Banska Stiavnica precious and base metal deposit, Slovakia—evidence from melt and fluid inclusions. ECONOMIC GEOLOGY, v. 94, p. 949–956.

Setterfield, T. H., Mussett, A.E, and Oglethorpe, R.D.J., 1992, Magmatism and associated hydrothemal activity during the evolution of the Tavua caldera: $^{40}Ar/^{39}Ar$ dating of the volcanic, intrusive, and hydrothermal events: ECONOMIC GEOLOGY, v. 87, p. 30–1140.

Shinohara, H., and Hedenquist, J.W., 1997, Constraints on magma degassing beneath the Far Southeast porphyry Cu-Au deposit, Phillipines: Journal of Petrology, v. 38, p. 1741–1752.

Silberman, M.L., 1985, Geochronology of hydrothermal alteration and mineralization: Tertiary epithermal precious-metal deposits in the Great Basin: U.S. Geological Survey Bulletin 1646, p. 55-70.

Sillitoe, R.H., 1989, Gold deposits in western Pacific island arcs: The magmatic connection: Economic Geology Monograph 6, p. 274–291.

——1995, Exploration of porphyry copper lithocaps: Australasian Institute of Mining and Metallurgy Publication Series 9/95, p. 527–532.

Singer, B.S., Hoffman, K.A., Chauvin, A., Coe, R.S. and Pringle, M.S., 1999, Dating transitionally magnetized lavas of the late Matuyama Chron: Toward a new ^{40}Ar/^{39}Ar timescale of reversals and events: Journal of Geophysical Research, v. 104, p. 679–693.

Yanev, Y., and Pĕcskay, Z., 1997, Preliminary data on the petrology and K-Ar dating of the Oligocene volcano Briastovo, Eastern Rhodopes. Bulgarian Academy of Sciences, Geochemistry Mineralogy and Petrology, v. 32, p. 59–66.

Yosifov, D., Maneva, B., Tsvetkov, A., Tsvetkova, D., and Pchelarov, B., 1990, Geotectonic position and structure of Spahievo ore field: Geologica Balcanica, v. 20/1, p. 45–65.

APPENDIX

Individual ^{40}Ar/^{39}Ar Laser-Fusion Analyses of 105 Sanidine, Biotite, K feldspar, Plagioclase, Adularia, and Alunite Samples

Sample	Experiment number	^{40}Ar/^{39}Ar	^{37}Ar/^{39}Ar[1]	^{36}Ar/^{39}Ar	^{40}Ar* (10^{-14} mole)	% ^{40}Ar*	K/Ca	Apparent age ± 2σ Ma[2]
	GE117X1A	1.954	0.00806	0.0019790	0.46	69.9	60.77	31.72 ± 0.28
224 sanidine	GE117X1B	1.576	0.00813	0.0006750	0.28	87.1	71.78	31.50 ± 0.42
J = 0.01299	GE117X1C	2.056	0.00682	0.0023544	0.24	66.0	60.30	31.87 ± 0.26
Post-Borovitsa caldera	GE117X1D	1.533	0.00680	0.0005455	0.60	89.2	72.09	31.79 ± 0.26
Quartz trachyte dike	GE117X1E	1.792	0.00790	0.0014577	0.31	75.7	62.03	31.53 ± 0.34
	GE117X1F	1.425	0.19639	0.0002238	0.14	96.1	2.49	31.81 ± 0.38
	GE117X1G	1.614	0.00761	0.0008168	0.46	84.8	64.35	31.79 ± 0.26
						Mean ± 2s		31.72 ± 0.42
						Weighted mean ± 2s		31.75 ± 0.32
						Isochron ± 2s		31.88 ± 0.38
	97GE815I	6.326	0.02246	0.0021475	9.37	89.9	21.81	30.75 ± 0.64
B86-37 biotite	97GE815G	6.603	0.04233	0.0028570	5.83	87.2	11.57	31.11 ± 0.70
J = 0.003022	97GE815E	6.318	0.01479	0.0015665	5.11	92.6	33.14	31.62 ± 0.64
Post-Borovitsa caldera	97GE815C	6.384	0.01802	0.0016504	6.75	92.3	27.19	31.84 ± 0.64
latite dike	97GE815D	6.530	0.03614	0.0020880	4.01	90.5	13.56	31.94 ± 0.66
	97GE815B	6.274	0.01767	0.0001177	9.70	94.7	27.73	32.10 ± 0.62
	97GE815A	6.256	0.02212	0.0009819	6.79	95.3	22.14	32.22 ± 0.60
						Mean ± 2s		31.66 ± 1.10
						Weighted mean ± 2s		31.76 ± 0.44
	GE116X4A	1.490	0.07366	0.0004246	0.22	91.7	6.65	31.63 ± 0.30
217A sanidine	GE116X4B	1.572	0.00874	0.0006393	0.25	87.7	56.06	31.94 ± 0.26
J = 0.01295	GE116X4C	1.646	0.00896	0.0008921	0.31	83.7	54.67	31.91 ± 0.30
Murga caldera	GE116X4D	1.520	0.00791	0.0004743	0.23	90.5	61.93	31.87 ± 0.32
rhyolite ring-dike	GE116X4E	1.525	0.01064	0.0005183	0.08	89.7	46.06	31.67 ± 0.50
	GE116X4F	1.548	0.01270	0.0005848	0.16	88.6	38.43	31.77 ± 0.36
	GE116X4G	1.491	0.01180	0.0003610	0.12	92.6	41.62	31.96 ± 0.46
	GE116X4I	1.387	0.00868	0.0006604	0.12	87.4	56.48	32.11 ± 0.52
	GE116X4J	1.558	0.00832	0.0005763	0.14	88.8	58.88	32.05 ± 0.42
	GE116X4K	1.614	0.00947	0.0008004	0.21	85.1	51.76	31.80 ± 0.36
						Mean ± 2s		31.87 ± 0.36
						Weighted mean ± 2s		31.86 ± 0.22
						Isochron ± 2s		31.67 ± 0.48
	97GE804H	6.025	3.31415	0.0018080	4.34	95.4	0.15	31.78 ± 1.16
Zd-95-1 plagioclase	97GE804F	5.831	0.12328	0.0001685	3.24	99.2	3.97	31.89 ± 0.94
J = 0.003082	97GE804G	6.888	3.31092	0.0046436	0.27	83.8	0.15	31.89 ± 1.36
Borovitsa tuff	97GE804A	5.831	0.30732	0.0001484	13.51	99.6	1.59	32.00 ± 0.58
						Mean ± 2s		31.89 ± 0.32
						Weighted mean ± 2s		31.93 ± 0.50
	GE117X2A	1.579	0.01602	0.0005525	0.52	89.5	30.59	*32.66 ± 0.22
S96-5 adularia	GE117X2B	2.140	0.00115	0.0025140	0.71	65.1	424.66	32.20 ± 0.34
Low-sulfidation	GE117X2C	1.850	0.00105	0.0015210	0.77	75.5	467.66	32.27 ± 0.30
alteration zone	GE117X2E	1.525	0.01552	0.0004074	0.54	91.9	31.57	*32.40 ± 0.26

APPENDIX

(Cont.)

Sample	Experiment number	$^{40}Ar/^{39}Ar$	$^{37}Ar/^{39}Ar^{1}$	$^{36}Ar/^{39}Ar$	$^{40}Ar^{*}$ (10^{-14} mole)	% $^{40}Ar^{*}$	K/Ca	Apparent age ± 2σ Ma[2]
	GE117X2F	1.659	0.01040	0.0008560	0.46	84.5	47.10	*32.42 ± 0.26
	GE117X2G	2.758	0.00184	0.0046320	0.81	50.2	265.74	32.00 ± 0.40
	GE117X2H	1.894	0.00135	0.0016860	0.45	73.5	363.54	32.16 ± 0.30
	GE117X2I	1.721	0.00210	0.0012060	0.64	80.5	233.28	32.03 ± 0.24
	GE117X2J	1.760	0.00232	0.0012440	1.18	78.9	211.35	32.08 ± 0.20
	GE117X2K	1.820	0.00279	0.0014390	0.59	76.4	175.89	32.13 ± 0.26
	GE117X2L	1.782	0.00135	0.0013110	0.65	78.0	364.21	32.13 ± 0.30
						Mean ± 2s		32.13 ± 0.20
						Weighted mean ± 2s		32.12 ± 0.14
						Isochron ± 2s		32.14 ± 0.20
	GE116X3A	1.513	0.01089	0.0004126	2.14	91.7	44.98	32.19 ± 0.14
BR-97-3 sanidine	GE116X3B	1.525	0.00951	0.0004385	1.70	91.2	51.50	32.26 ± 0.18
J = 0.01297	GE116X3E	1.512	0.01459	0.0004150	1.36	91.7	33.59	32.14 ± 0.16
Borovitsa pyroclastic	GE116X3F	1.965	1.89095	0.0023734	0.12	71.7	0.26	*32.71 ± 0.52
flow	GE116X3G	1.489	0.00763	0.0003258	1.17	93.3	64.26	32.19 ± 0.20
	GE116X3H	1.459	0.00728	0.0002135	1.11	95.4	67.27	32.25 ± 0.20
	GE116X3I	1.474	0.00676	0.0002941	1.19	93.8	72.49	32.08 ± 0.16
	GE116X3J	1.472	0.00666	0.0002737	1.94	94.2	73.54	32.17 ± 0.16
	GE116X3K	1.505	0.00980	0.0003999	2.05	91.9	49.99	32.06 ± 0.18
						Mean ± 2s		32.17 ± 0.34
						Weighted mean ± 2s		32.16 ± 0.30
						Isochron ± 2s		32.17 ± 0.42
	GE116X2A	1.428	0.00630	0.0001269	4.96	97.4	77.73	32.19 ± 0.16
BR-97-2 sanidine	GE116X2B	1.516	0.00077	0.0004136	1.17	91.7	63.32	32.18 ± 0.20
J = 0.01295	GE116X2C	1.446	0.00700	0.0001779	1.26	96.0	69.96	32.16 ± 0.20
Mineralni Bani	GE116X2D	1.439	0.00694	0.0001523	1.34	96.6	70.65	32.17 ± 0.20
rhyolite dome	GE116X2E	1.443	0.00705	0.0001727	0.09	96.2	69.51	32.13 ± 0.16
	GE116X2F	1.538	0.00818	0.0004924	0.01	90.3	59.92	32.16 ± 0.22
	GE116X2G	1.523	0.07946	0.0004576	1.08	91.2	6.17	32.18 ± 0.20
	GE116X2I	1.451	0.00729	0.0001958	1.64	95.7	67.20	32.16 ± 0.20
						Mean ± 2s		32.17 ± 0.26
						Weighted mean ± 2s		32.17 ± 0.26
						Isochron ± 2s		32.16 ± 0.30
	GE115X3A	1.403	0.01472	0.0000275	0.10	99.2	33.28	32.36 ± 0.16
S96-11 sanidine	GE115X3B	1.602	0.01387	0.0007209	0.58	86.5	35.36	32.24 ± 0.24
J = 0.01301	GE115X3C	1.449	0.01749	0.0001968	0.63	95.8	28.01	32.27 ± 0.20
Mineralni Bani	GE115X3D	1.415	0.01465	0.0000917	0.63	97.8	33.45	32.21 ± 0.20
latite lava flow	GE115X3E	1.415	0.01378	0.0000581	0.13	98.5	35.56	32.44 ± 0.36
	GE115X3F	1.409	0.01429	0.0000642	0.64	98.4	34.29	32.26 ± 0.20
	GE115X3G	1.434	0.01508	0.0001301	0.61	97.1	32.50	32.40 ± 0.20
	GE115X3H	1.404	0.01311	0.0000447	0.86	98.8	37.38	32.26 ± 0.18
						Mean ± 2s		32.30 ± 0.28
						Weighted mean ± 2s		32.30 ± 0.24
						Isochron ± 2s		32.31 ± 0.24
	97GE806E	6.073	0.01252	0.0005416	7.81	97.3	34.07	32.48 ± 0.54
S96-4 sanidine	97GE806A	6.219	0.01437	0.0009604	27.88	95.4	34.08	32.61 ± 0.48
J = 0.003075	97GE806F	6.012	0.01268	0.0002361	16.46	98.8	39.30	32.65 ± 0.46
Precaldera, high K	97GE806C	6.014	0.01228	0.0001829	28.75	99.0	38.52	32.74 ± 0.52
lava flow	97GE806D	6.088	0.01337	0.0004280	17.28	97.9	36.64	32.75 ± 0.48
	97GE806B	6.048	0.01570	0.0002783	23.58	98.6	31.30	32.78 ± 0.46
	97GE806G	6.304	0.01119	0.0010356	15.12	95.1	43.80	32.95 ± 0.50
						Mean ± 2s		32.71 ± 0.40
						Weighted mean ± 2s		32.72 ± 0.32

APPENDIX

(Cont.)

Sample	Experiment number	$^{40}Ar/^{39}Ar$	$^{37}Ar/^{39}Ar$[1]	$^{36}Ar/^{39}Ar$	$^{40}Ar^*$ (10^{-14} mole)	% $^{40}Ar^*$	K/Ca	Apparent age ± 2σ Ma[2]
	97GE816B	7.314	0.00219	0.0041544	0.05	83.2	224.20	32.81 ± 0.58
208 biotite	97GE816C	6.821	0.00589	0.0023780	1.16	89.6	83.16	32.99 ± 0.20
J = 0.003018	97GE816D	6.691	0.00738	0.0021630	0.08	90.4	66.37	32.63 ± 0.22
Precaldera lava flow	97GE816E	6.438	0.00673	0.0012166	2.14	94.4	72.81	32.77 ± 0.12
						Mean ± 2s		32.80 ± 0.40
						Weighted mean ± 2s		32.79 ± 0.30
	GE115X4A	4.330	0.13093	0.0099186	0.20	32.4	3.74	32.70 ± 0.86
S96-2b alunite	GE115X4B	2.776	0.03416	0.0046706	0.30	50.2	14.34	32.46 ± 0.58
J = 0.01302	GE115X4C	2.706	0.04405	0.0043839	0.14	52.1	11.12	32.80 ± 0.58
High-sulfidation	GE115X4F	4.034	0.11803	0.0088345	0.13	35.4	4.15	33.23 ± 0.68
alteration zone	GE115X4I	2.786	0.04695	0.0045954	0.15	51.2	10.43	33.21 ± 0.72
	GE115X4J	3.224	0.04776	0.0059984	0.08	45.0	10.26	33.76 ± 0.94
	GE115X4K	3.838	0.08524	0.0080427	0.07	38.1	5.75	34.05 ± 1.40
	GE115X4L	3.111	0.06927	0.0057768	0.14	45.2	7.07	32.70 ± 0.92
	GE115X4M	3.718	0.10560	0.0078243	0.12	37.9	4.64	32.82 ± 0.98
	GE115X4N	2.689	0.03350	0.0043753	0.35	51.8	14.62	32.44 ± 0.62
	GE116X1C	3.243	0.06733	0.0062387	0.09	43.2	7.29	32.60 ± 1.08
	GE116X1B	2.783	0.05277	0.0047076	0.15	50.0	9.28	32.39 ± 0.66
	GE116X1A	2.621	0.03882	0.0004005	0.06	54.8	12.62	33.42 ± 1.18
						Mean ± 2s		32.82 ± 1.06
						Weighted mean ± 2s		32.82 ± 0.40
	97GE8141	6.688	0.03521	0.0021216	1.60	27.4	13.91	32.84 ± 0.16
S96-1 Biotite	97GE8142	6.815	0.03481	0.0025506	0.79	13.6	14.08	32.84 ± 0.24
J = 0.003032	97GE8143	7.531	0.03832	0.0050234	0.96	16.5	12.79	32.77 ± 0.22
Sarnitsa monzonite	97GE8144	6.690	0.05498	0.0023584	0.86	15.0	8.91	32.49 ± 0.22
intrusion	97GE8145	6.981	0.14636	0.0030349	0.76	13.0	33.48	32.96 ± 0.22
	97GE8146	6.903	0.04236	0.0028474	0.84	14.5	11.56	32.85 ± 0.20
						Mean ± 2s		32.85 ± 0.30
						Weighted mean ± 2s		32.85 ± 0.28
	97GE805A	6.086	0.02222	0.0003370	6.05	98.3	22.05	32.92 ± 0.48
S96-1 K feldspar	97GE805C	6.163	0.03460	0.0001452	12.75	99.3	14.15	33.66 ± 0.52
J = 0.003078	97GE805D	6.151	0.02948	0.0004616	18.45	97.7	16.62	33.08 ± 0.52
Sarnitsa monzonite	97GE805E	6.127	0.02420	0.0005660	9.24	97.2	20.25	32.78 ± 0.62
intrusion	97GE805F	6.191	0.02860	0.0008210	7.80	96.0	17.10	32.72 ± 0.64
	97GE805G	6.229	0.02340	0.0009301	12.02	95.5	20.89	32.74 ± 0.64
	97GE805H	6.260	0.02930	0.0011764	6.43	94.4	16.75	32.52 ± 0.64
						Mean ± 2s		32.92 ± 0.78
						Weighted mean ± 2s		32.99 ± 0.38

Notes: Samples were from the Spaheivo area, Rhodope Mountains, Bulgaria; samples were single or multi-crystal, between 0.1 and 1.0 mg
Reactor corrections: $^{36}Ar/^{37}Ar(Ca)$ = 0.0000268, $^{39}Ar/^{37}Ar(Ca)$ = 0.000698, and $^{40}Ar/^{39}Ar(K)$ = 0.0465
$\lambda_E = 0.58 \times 10^{-10}$/yr; $\lambda_B = 4.692 \times 10^{-10}$/yr; weighting for weighted means is by the inverse of the variance; preferred ages in bold type
[1] Corrected for ^{37}Ar and ^{39}Ar decay, half-lives of 35 days and 259 years, respectively
[2] Ages calculated relative to TCR-sanidine (27.92 Ma; Duffield and Dalrymple, 1990; see text), ± 2σ errors
*Indicates outlier; analysis excluded from mean and weighted mean calculations